Electronic Supplementary Material (ESI) for Inorganic Chemistry Frontiers.

A Pd_3L_6 Supramolecular Cage Incorporating Photoactive [2.2]Paracyclophane Units

*Diego Rota Martir,[a] Lucie Delforce,[a] David B. Cordes,[a] Alexandra M. Z. Slawin,[a] Stuart L. Warriner,[b] Denis Jacquemin,[c] and Eli Zysman-Colman[a]**

[a]Organic Semiconductor Centre, EaStCHEM School of Chemistry, University of St Andrews, St Andrews, Fife, KY16 9ST, UK, Fax: +44-1334 463808; Tel: +44-1334 463826; E-mail: eli.zysman-colman@st-andrews.ac.uk;
URL: http://www.zysman-colman.com
[b]School of Chemistry, University of Leeds, Woodhouse Lane, Leeds, LS2 9JT, UK.
[c]CESIAM Laboratory, UMR CNRS 6230, University of Nantes, 2, rue de la Houssinière, 44322 Nantes, Cedex 3, France.

SUPPORTING INFORMATION

Table of Contents:

Experimental section.

General Synthetic Procedures. Commercial chemicals were used as supplied. All reactions in the synthesis of the ligands and cages were performed using standard Schlenk techniques under inert (N_2) atmosphere with reagent-grade solvents. Flash column chromatography was performed using silica gel (Silia-P from Silicycle, 60 Å, 40-63 μm). Analytical thin layer chromatography (TLC) was performed with silica plates with aluminum backings (250 μm with indicator F-254). Compounds were visualized under UV light. ^{1}H (including ^{1}H DOSY), and ^{13}C solution-phase NMR spectra were recorded on a Bruker Avance spectrometer operating at 11.7 T (Larmor frequencies of 400, 126 and 500 MHz, respectively). The following abbreviations have been used for multiplicity assignments: "s" for singlet, "d" for doublet, "t" for triplet, "m" for multiplet and "br" for broad.

General procedure for the synthesis of **pCpd3py** and **pCpd4py**: 7-15-dibromocyclophene (4.0 g, 16.74 mmol, 1 equiv.), 3- or 4-pyridinylboronic acid (5.1 g, 41.90 mmol, 2.5 equiv.) and potassium carbonate (50 mmol) were added to a round-bottom flask containing 50 mL of a mixture of 1,4-dioxane and distilled water (4:1 v/v). The reaction mixture was degassed by multiple vacuum and N_2 purging cycles, and $Pd(PPh_3)_4$ (0.693 g, 0.60 mmol, 0.03 equiv.) was added to the flask under positive nitrogen pressure. The mixture was heated at reflux under a nitrogen atmosphere for 48 h and then cooled to room temperature. The mixture was poured into distilled water (30 mL) and extracted three times with DCM (20 mL each extraction). The organic fractions were combined, washed with a portion of brine and dried over magnesium sulfate. Filtration and evaporation under reduced pressure gave the crude product as a brown solid (3.80 g). The crude product was purified by flash column chromatography (dichloromethane on silica) to afford the pure compound as a white solid.

pCp3py: White solid. **Yield:** 51%. **R*f*:** 0.48 (6% MeOH/DCM). **^{1}H NMR (400 MHz, $CDCl_3$):** δ (ppm) 8.60 (dd, *J* = 2.5 Hz, 0.8 Hz, 2H), 8.59 (dd, *J* = 4.9 Hz, 1.7 Hz, 2H), 7.60 (ddd, *J* = 7.9 Hz, 2.4 Hz, 1.6 Hz, 2H), 7.34 (ddd, *J* = 7.9 Hz, 4.8 Hz, 0.9 Hz, 2H), 6.78 (d, *J* = 7.7 Hz, 2H), 6.71 (dd, *J*

= 7.7 Hz, 1.9 Hz, 2H), 6.61 (d, *J* = 1.9 Hz, 2H), 3.47 (ddd, *J* = 13.6 Hz, 10.0 Hz, 1.8 Hz, 2H), 3.17 (ddd, *J* = 12.7 Hz, 10.7 Hz, 1.7 Hz, 2H), 3.02 (ddd, *J* = 13.7 Hz, 10.4 Hz, 6.4 Hz, 2H), 2.74 (ddd, *J* = 13.3 Hz, 10.0 Hz, 6.5 Hz, 2H).**^{13}C NMR (126 MHz, DMSO-d_6):** δ (ppm) 149.19, 147.92, 139.60, 136.95, 136.45, 135.89, 135.85, 133.16, 129.50, 123.62, 33.84, 33.36. **^{1}H DOSY NMR (500 MHz, DMSO-*d_6*)** D (m^2/s): 2.5 × 10^{-10} m^2/s. **HR-MS (HR-NSI-MS): Calculated** ($C_{26}H_{23}N_2$): 363.1856 **Found:** 363.1857. **Elemental analysis:** Calculated for $C_{26}H_{22}N_2$: C, 86.15; H, 6.12; N, 7.73. Found: C, 86.31; H, 6.09; N, 7.66.

pCp4py: White solid. **Yield:** 72%. **R*f*:** 0.32 (5% EtOH/DCM). **^{1}H NMR (400 MHz, $CDCl_3$):** δ (ppm)8.63 (dd, *J* = 4.5 Hz, 1.7 Hz, 4H), 7.20 (dd, *J* = 4.5 Hz, 1.6 Hz, 4H), 6.77 (d, *J* = 7.7 Hz, 2H), 6.72 (dd, *J* = 7.7 Hz, 1.8 Hz, 2H), 6.63 (d, *J* = 1.8 Hz, 2H), 3.53 (ddd, *J* = 13.7 Hz, 10.1 Hz, 1.9 Hz, 2H), 3.19 (ddd, *J* = 12.6 Hz, 10.6 Hz, 1.6 Hz, 2H), 3.04 (ddd, *J* = 13.7 Hz, 10.4 Hz, 6.2 Hz, 2H), 2.80 (ddd, *J* = 13.1 Hz, 10.0 Hz, 6.2 Hz, 2H). **^{13}C NMR (126 MHz, DMSO-d_6):** δ (ppm) 149.92, 147.65, 139.69, 137.22, 137.12, 136.04, 133.76, 129.44, 127.39, 123.48, 33.82, 33.39. **^{1}H DOSY NMR (500 MHz, DMSO-*d_6*)** D (m^2/s): 2.5 × 10^{-10} m^2/s. **HR-MS (HR-NSI-MS): Calculated** ($C_{26}H_{23}N_2$): 363.1856 **Found:** 363.1857. **Elemental analysis:** Calculated for $C_{26}H_{22}N_2$: C, 86.15; H, 6.12; N, 7.73. Found: C, 86.14; H, 6.25; N, 7.70.

General procedure for the synthesis of cage **pCpd4py-Pd**. In a dry 10 mL Schlenk vial, the ligand **pCpd4py** (2 equiv.) and $[Pd(NCMe)_4](BF_4)_2$ (1 equiv.) were dissolved in DMSO-*d_6* (1 mL) to give a **pCpd4py** concentration of approximately 0.05 M. The solution was degassed for five minutes by bubbling nitrogen, then heated at 85 °C for 12 h under a nitrogen atmosphere. The solution was cooled to room temperature and the black solid was filtered through celite. A 2M MeOH/H_2O solution (1:1 v/v) of KBF_4 (5 mL) was added to the resulting DMSO solution and the mixture was stirred at room temperature for 4h. The solution was cooled in an ice bath for 30 minutes and the obtained precipitate was filtered and washed with water and diethyl ether. The self-assembly of **pCpd4py** with

$[Pd(NCMe)_4](BF_4)_2$ yielded pure **pCpd4py-Pd** as a yellow solid. $[(\mathbf{pCpd4py})_6Pd_3](BF_4)_6$, **(pCpd4py-Pd)*:* Yield: 90%**. **Mp:** 295 - 300˚C (degraded). **^{1}H NMR (500 MHz, DMSO-*d*$_6$) δ(ppm):** δ 9.35 (bs, 24H), 8.92 (bs, 24H), 7.54 (bs, 24H), 8.84 - 6.79 (m, 12H), 6.75 - 6.68 (m, 12H), 6.62 (bs, 12H), 6.42 (bs, 12H). **^{1}H DOSY NMR (500 MHz, DMSO-*d*$_6$)** D (m^2/s): 9.2×10^{-11} m^2/s. **HR ESI-MS: $[M\text{-}BF_4]^+$ Calculated:** $[(C_{26}H_{22}N_2)_6Pd_3(BF_4)_1]^{5+}$: 516.1577 Found: 516.1586; $[(C_{26}H_{22}N_2)_6Pd_3(BF_4)_2]^{4+}$: 666.6981 Found: 666.6988; $[(C_{26}H_{22}N_2)_6Pd_3(BF_4)_3]^{3+}$: 917.9323 Found: 917.9332; $[(C_{26}H_{22}N_2)_6Pd_3(BF_4)_4]^{2+}$: 1420.4005 Found: 1420.4015; $[(C_{26}H_{22}N_2)_6Pd_3(BF_4)_5]^{1+}$: 2927.8052 Found: 2927.8364.

^{1}H NMR and ^{1}H DOSY NMR of pCpd3py, pCpd4py and pCpd4py-Pd.

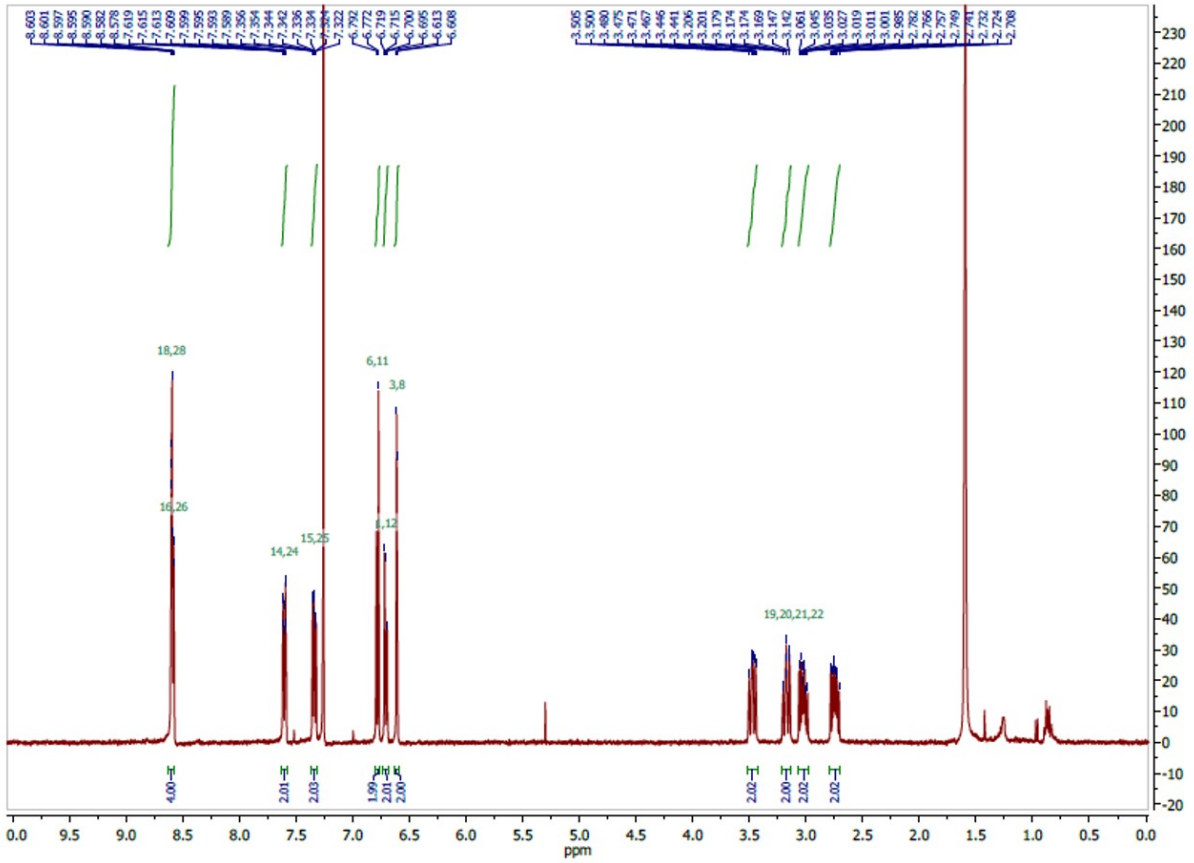

Figure **S1.**[1]H NMR spectrum of **pCpd3py** in $CDCl_3$.

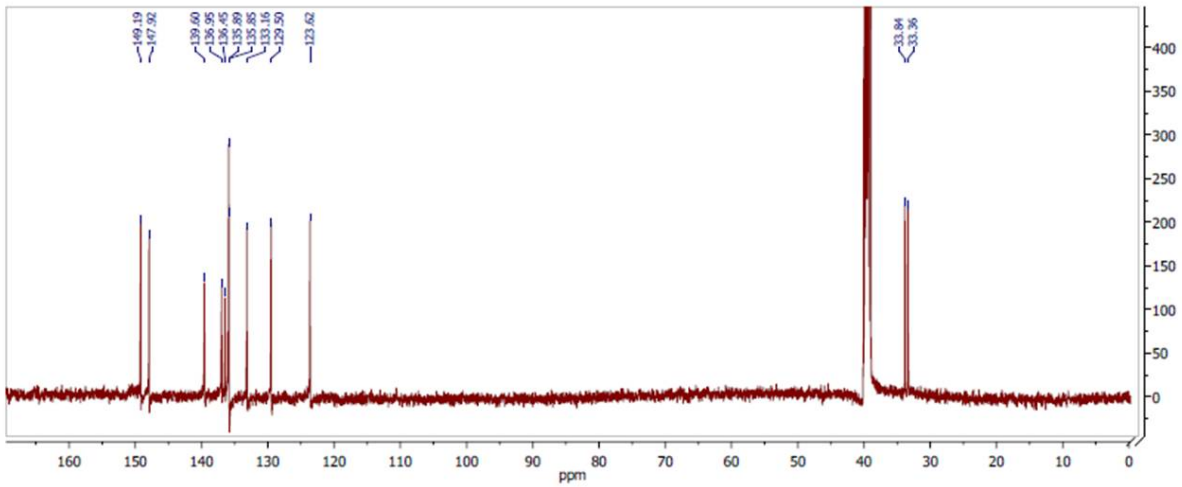

Figure **S2.** [13]C NMR spectrum of **pCpd3py** in DMSO-d_6.

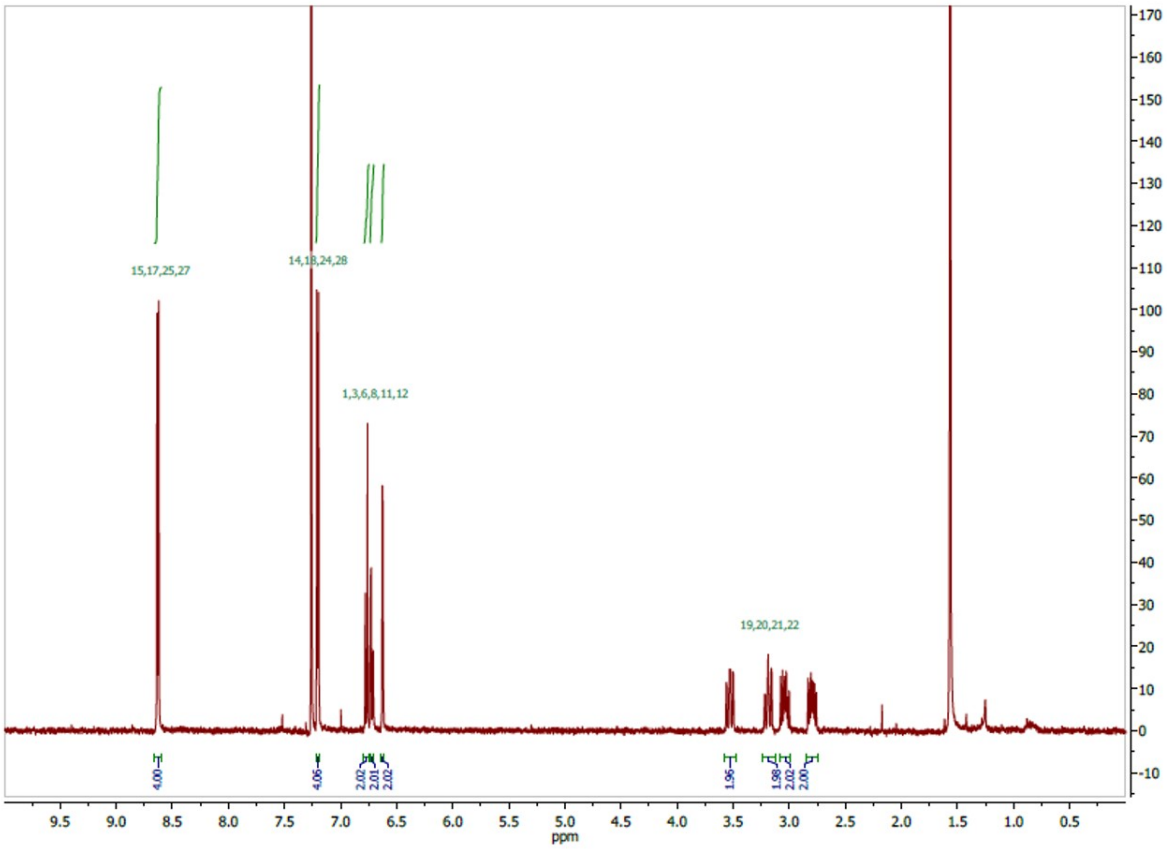

Figure **S3.**[1]H NMR spectrum of **pCpd4py** in $CDCl_3$.

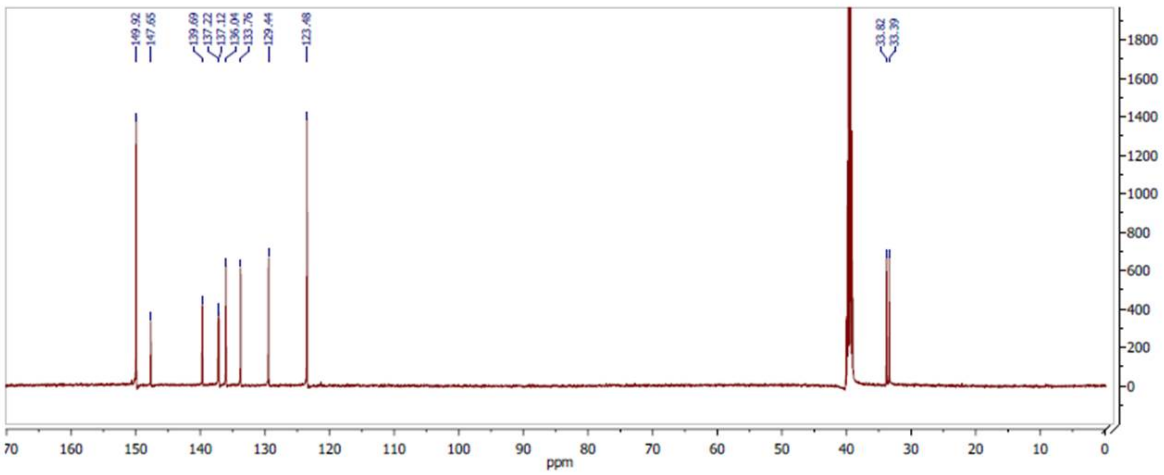

Figure **S4.** ^{13}C NMR spectrum of **pCpd4py** in DMSO-d_6.

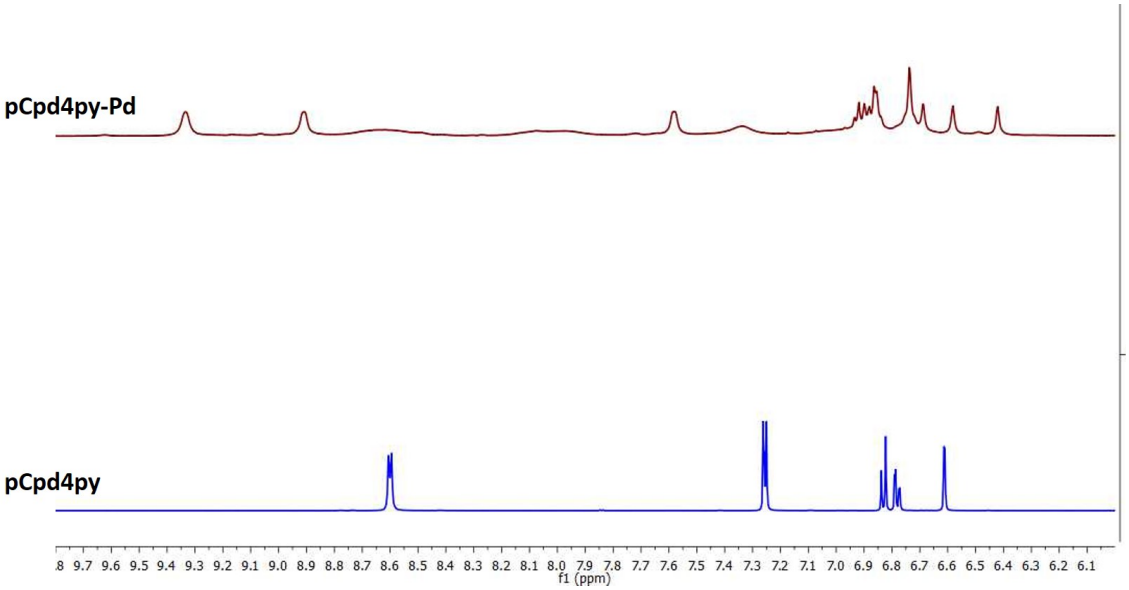

Figure **S5**.^{1}H NMR spectrum of **pCpd4py** (in blue), **pCpd4py-Pd** (in red) collected in DMSO-d_6 at 298 K.

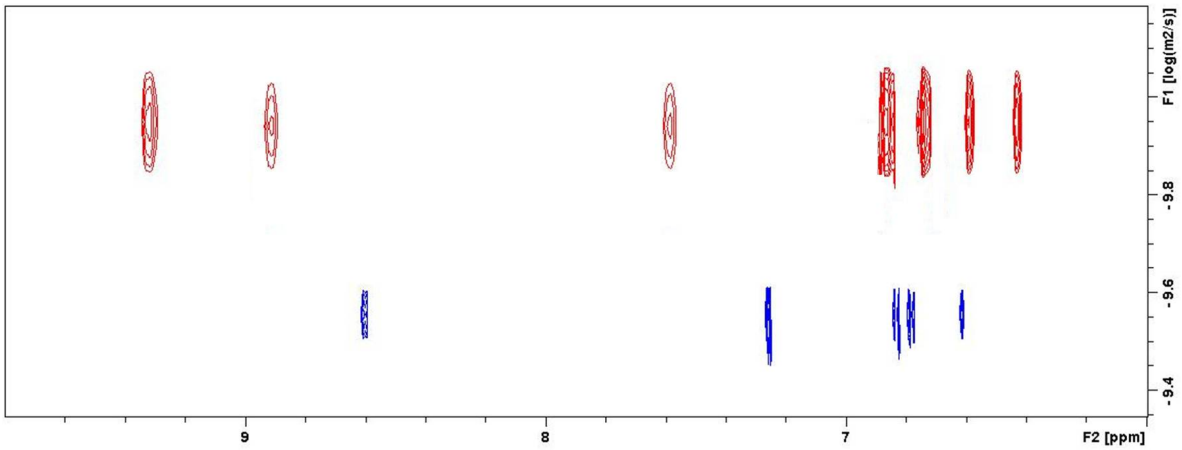

Figure **S6**.[1]H DOSY NMR spectrum of **pCpd4py** (in blue, $D = 2.5 \times 10^{-10}$ m^2/s), **pCpd4py-Pd** (in red, $D = 9.2 \times 10^{-11}$ m^2/s) collected in DMSO-d_6 at 298 K

Calculation of Hydrodynamic Radii (r_s) of pCp4py and pCp4py-Pd.

Table **S1.** Comparison of diffusion coefficients (D, m^2 s^{-1}) of ligand and cage obtained by ^{1}H DOSY NMR (500 MHz, DMSO-d_6).

ligand	**D metalloligand (m^2 s^{-1})**	**cages**	**D, cages (m^2 s^{-1})**	**r_s ligands (nm)**	**r_s cages (nm)**
pCpd4py	2.5×10^{-10}	**pCp4py-Pd**	9.1×10^{-11}	0.68	1.2

In diffusion experiments, the molecular size of the ligands and metallocages are estimated by the Stokes-Einstein equation:

$$r_s = \frac{k_b \cdot \mathrm{T}}{6\pi \cdot \eta \cdot D}$$

With r_s = hydrodynamic or Stokes radii of the ligands or metallocage, which are assumed to exhibit a spherical shape, k_b = Boltzmann constant, T = temperature (298 K), η = viscosity of DMSO solution (1.99 mPa · s) and D = diffusion coefficient, obtained here by ^{1}H DOSY NMR.

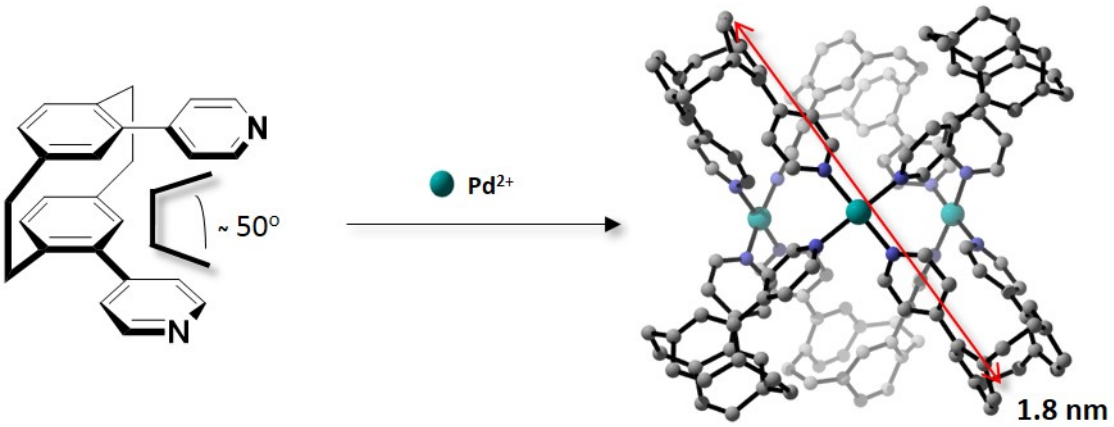

Figure **S7**. Illustration of the coordinating vector of **pCpd4py** and of the diameter of **pCpd4py-Pd** corresponding to the long axes of the structure. The structure of **pCpd4py-Pd** was obtained from X-ray diffraction.

HR-ESI-MS of pCp3py, pCp4py and cage pCp4py-Pd.

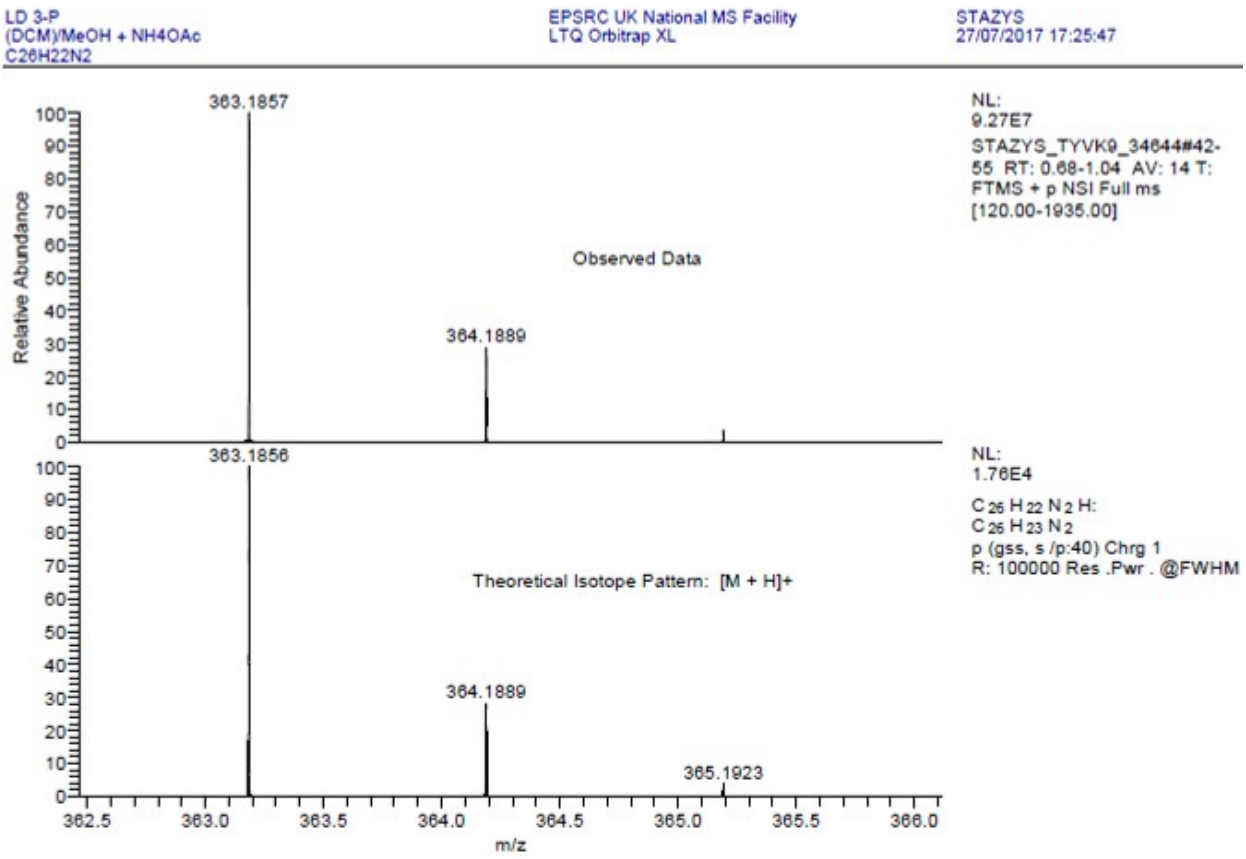

Figure **S8.** HR-MS spectra of **pCpd3py**.

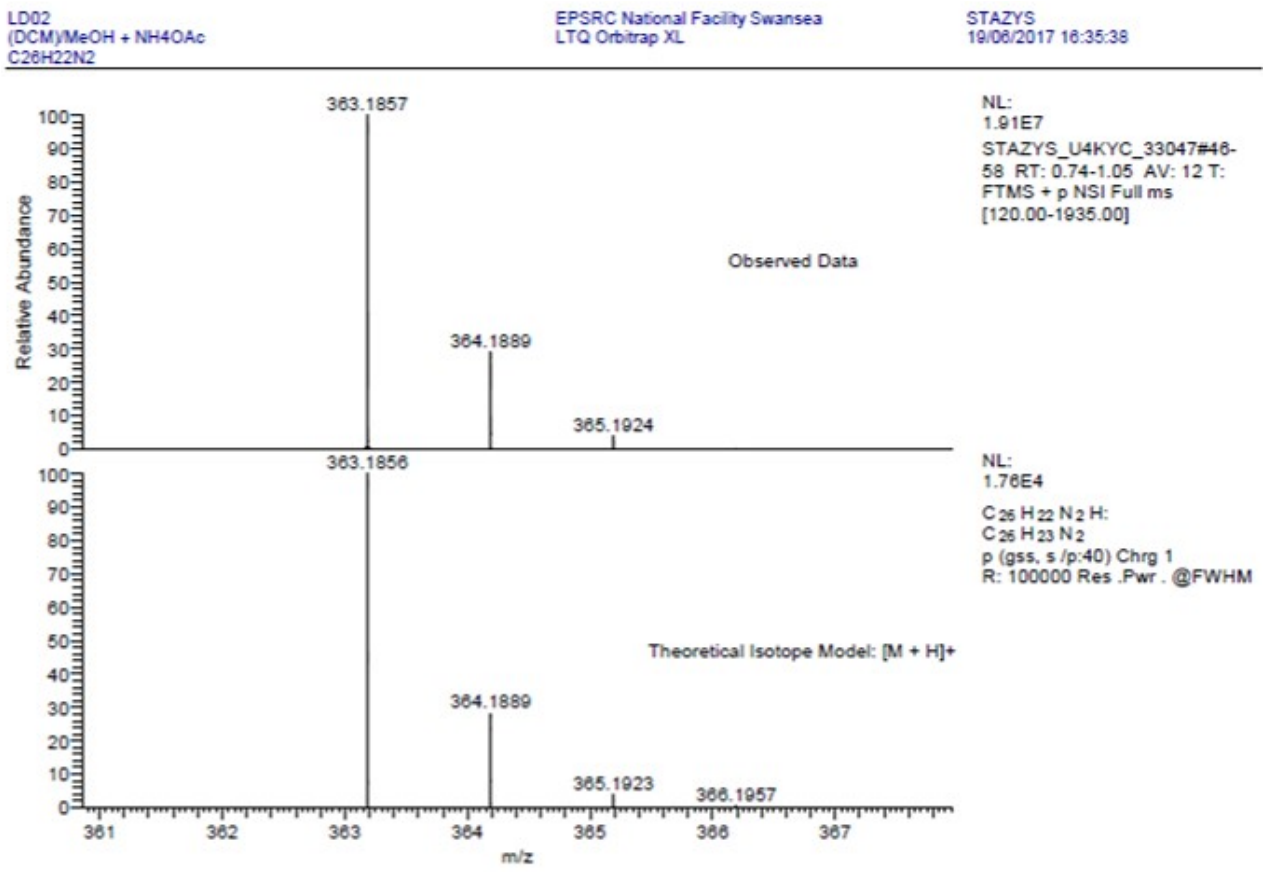

Figure **S9.** HR-MS spectra of **pCpd4py**.

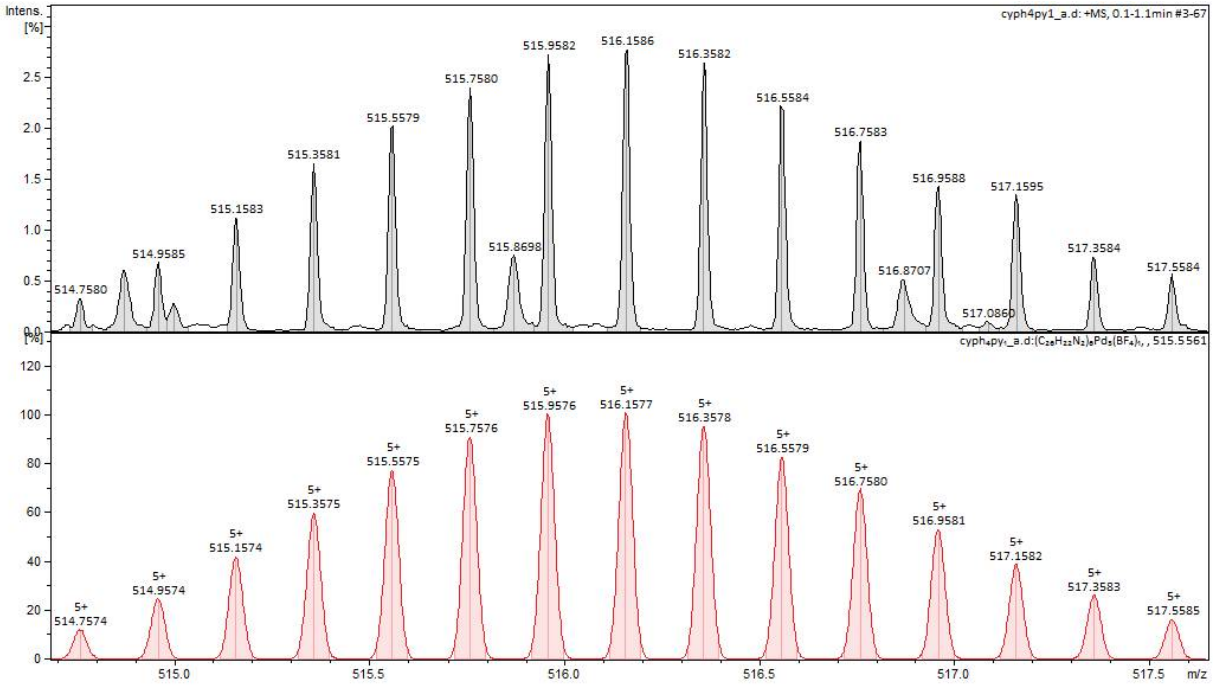

Figure **S10**. ESI-MS spectra of the [**pCpd4py-Pd**-$(BF_4)_5$]$^{5+}$ of (in black) and simulation of isotopic distribution pattern of [**pCpd4py-Pd** -$(BF_4)_5$]$^{5+}$ (in red).

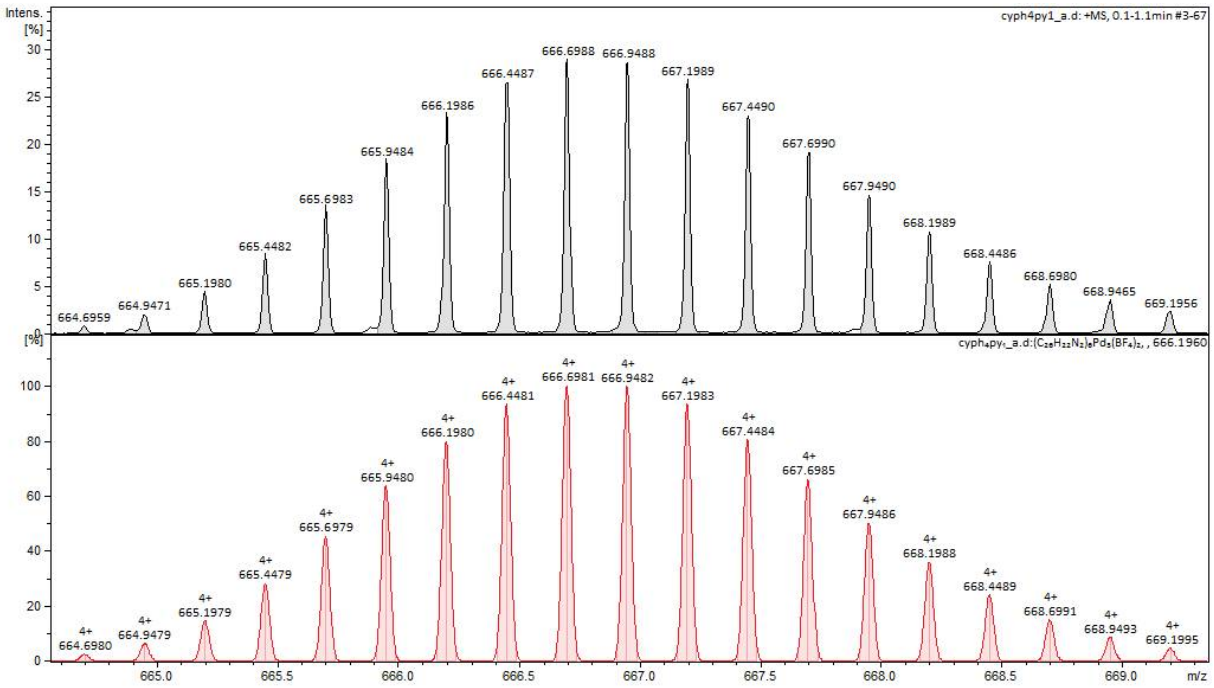

Figure **S11**. ESI-MS spectra of the [**pCpd4py-Pd**-$(BF_4)_4$]$^{4+}$ of (in black) and simulation of isotopic distribution pattern of [**pCpd4py-Pd** -$(BF_4)_4$]$^{4+}$ (in red).

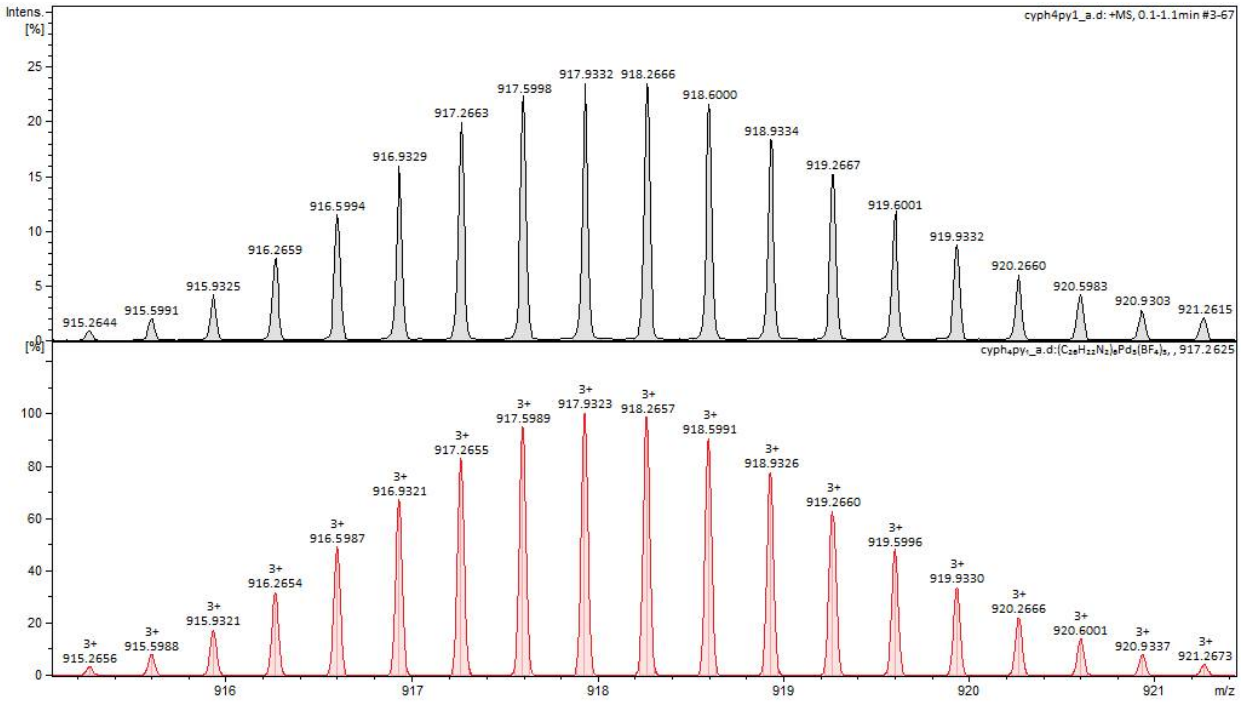

Figure **S12**. ESI-MS spectra of the [**pCpd4py-Pd**-$(BF_4)_3$]$^{3+}$ of (in black) and simulation of isotopic distribution pattern of [**pCpd4py-Pd** -$(BF_4)_3$]$^{3+}$ (in red).

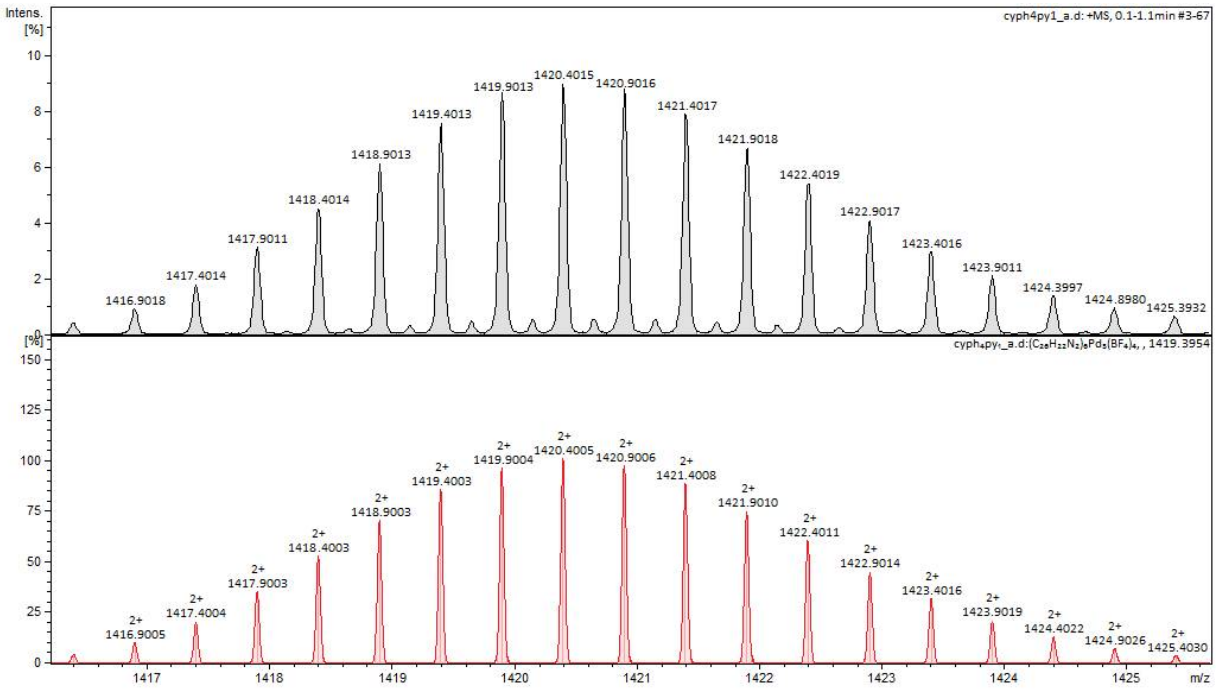

Figure **S13**. ESI-MS spectra of the [**pCpd4py-Pd**-$(BF_4)_2$]$^{2+}$ of (in black) and simulation of isotopic distribution pattern of [**pCpd4py-Pd** -$(BF_4)_2$]$^{2+}$ (in red).

X-ray crystallography.

X-ray diffraction data for **pCpd3py**, **pCpd4py** and **pCpd4py-Pd** were collected at 173 K using a Rigaku FR-X Ultrahigh Brilliance Microfocus RA generator/confocal optics with XtaLAB P200 diffractometer [Mo Kα radiation (λ = 0.71075 Å)]. Intensity data were collected using ω steps accumulating area detector images spanning at least a hemisphere of reciprocal space. Data for all compounds were collected using CrystalClear[1] and processed (including correction for Lorentz, polarization and absorption) using either CrystalClear[1] or CrysAlisPro.[2] Structures were solved by either direct (SIR2011)[3] or dual-space (SHELXT-2014/5)[4] methods and refined by full-matrix least-squares against F^2 (SHELXL-2018/3).[5] Non-hydrogen atoms were refined anisotropically, and hydrogen atoms were refined using a riding model. Only one of the two BF_4^- anions necessary for charge-balance could be located in the asymmetric unit of the structure of **pCpd4py-Pd**, which

additionally showed high proportions of void space (3783 Å^3). The SQUEEZE[6] routine implemented in PLATON[7] was used to remove the contribution of the unordered electron density in the void spaces, including that of the anions. The second BF_4^- anion has been included in the formula, formula weight, calculated density, μ, and F(000). All calculations except SQUEEZE were performed using the CrystalStructure[8] interface. Selected crystallographic data are presented in Table **S1**. Thermal ellipsoid plots for the three structures are presented in Figures **S14-S16**. CCDC 1951959-1951961 contains the supplementary crystallographic data for this paper. The data can be obtained free of charge from The Cambridge Crystallographic Data Centre via www.ccdc.cam.ac.uk/structures.

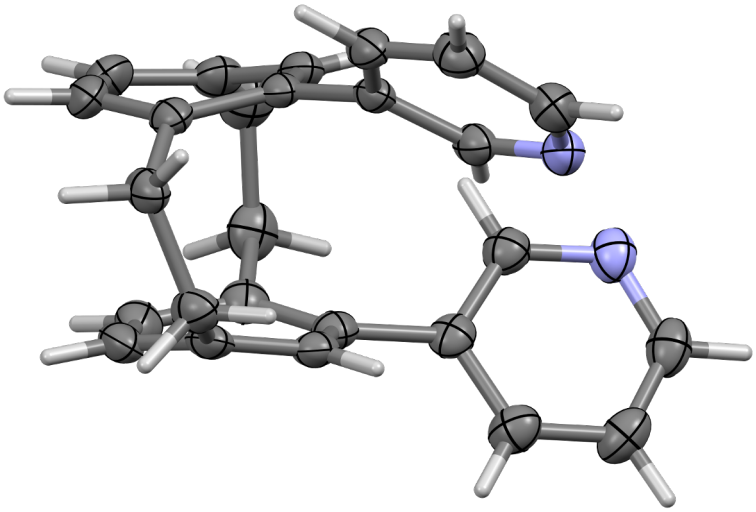

Figure **S14**. X-ray structure of **pCpd3py**, thermal ellipsoids are drawn at the 50% probability level.

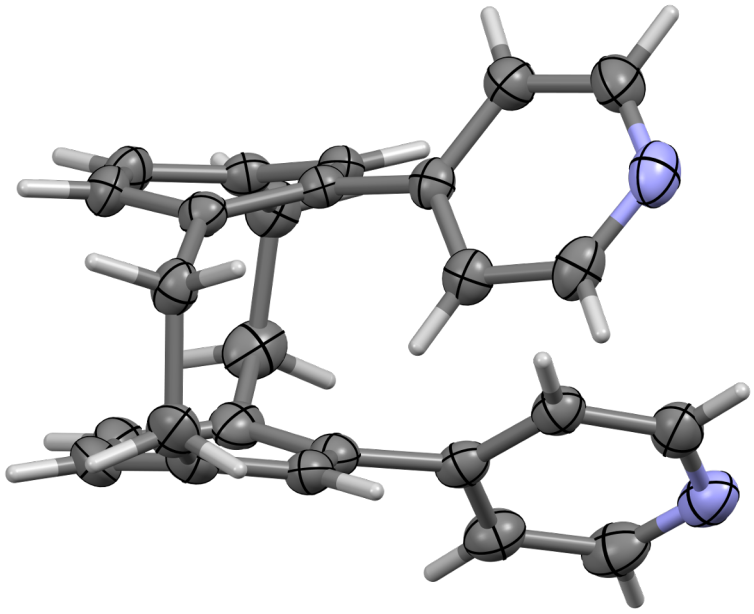

Figure **S15**. X-ray structure of **pCpd4py**, thermal ellipsoids are drawn at the 50% probability level.

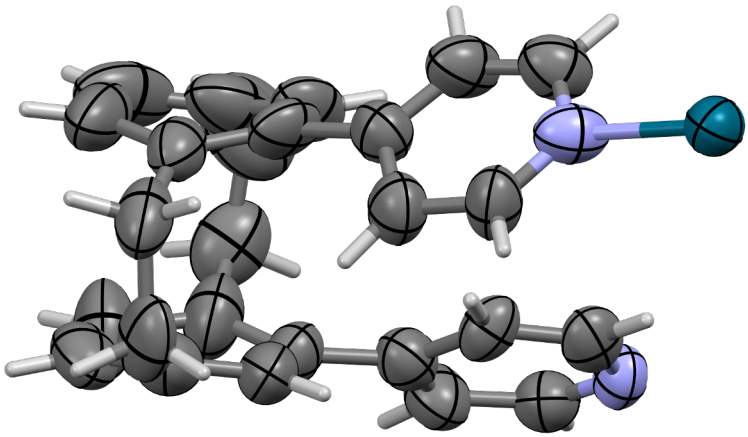

Figure **S16**. The asymmetric unit of the X-ray structure of **pCpd4py-Pd**, thermal ellipsoids are drawn at the 50% probability level, and anions are omitted for clarity.

Table **S1**. Selected crystallographic data.

	pCpd4py	**pCpd4py**	**pCpd4py-Pd**
empirical formula	$C_{26}H_{22}N_2$	$C_{26}H_{22}N_2$	$C_{156}H_{132}B_6F_{24}N_{12}Pd_3$
fw	362.47	362.47	3014.86
crystal description	colourless prism	colourless prism	colourless prism
crystal size [mm^3]	0.26×0.09×0.04	0.25×0.10×0.08	0.09×0.07×0.04
space group	*Pbca*	$P2_1/c$	*R*32
a [Å]	12.2170(13)	10.8591(18)	16.0519(12)
b [Å]	13.2161(15)	9.4365(15)	
c [Å]	23.200(3)	18.529(4)	55.296(4)
β [°]		93.737(4)	
vol [$Å^3$]	3745.9(8)	1894.7(6)	12339(2)
Z	8	4	3
ρ (calc) [g/cm^3]	1.285	1.271	1.217
μ [mm^{-1}]	0.075	0.074	0.401
F(000)	1536	768	4608
reflns collected	43250	22348	54308
independent reflns (R_{int})	3438 (0.0413)	3470 (0.0329)	6604 (0.1885)
data/restraints/ params	3438/0/253	3470/0/253	6604/3/286
GoF on F^2	1.034	1.027	0.931
R_1 [$I > 2\sigma(I)$]	0.0370	0.0390	0.0720
wR_2 (all data)	0.0937	0.1017	0.2085
largest diff. peak/hole [$e/Å^3$]	0.17, -0.16	0.21, -0.17	0.82, -0.31

Optoelectronic Characterization.

Photophysical measurements. All samples were prepared in HPLC grade DCM with varying concentrations on the order of 10^{-4}-10^{-6} M. The sample solutions for the emission spectra were prepared in HPLC-grade DCM and degassed *via* freeze-pump-thaw cycles using a quartz cuvette designed in-house. Steady-state emission and excitation spectra and time-resolved emission spectra were recorded at 298 K using an Edinburgh Instruments F980. All samples for steady-state measurements were excited at 360 nm using a xenon lamp, while samples for time-resolved measurements were excited at 378 nm using a PDL 800-D pulsed diode laser. Photoluminescence

quantum yields were determined using the optically dilute method.[9] A stock solution with absorbance of *ca*. 0.5 was prepared and then four dilutions were prepared with dilution factors between 2 and 20 to obtain solutions with absorbances of *ca*. 0.095, 0.065, 0.05 and 0.018, respectively. The Beer-Lambert law was found to be linear at the concentrations of these solutions. The emission spectra were then measured after the solutions were rigorously degassed *via* three freeze-pump-thaw cycles prior to spectrum acquisition. For each sample, linearity between absorption and emission intensity was verified through linear regression analysis and additional measurements were acquired until the Pearson regression factor (R^2) for the linear fit of the data set surpassed 0.9. Individual relative quantum yield values were calculated for each solution and the values reported represent the slope value. The equation $\Phi_s = \Phi_r(A_r/A_s)(I_s/I_r)(n_s/n_r)^2$ was used to calculate the relative quantum yield of each of the sample, where Φ_r is the absolute quantum yield of the reference, n is the refractive index of the solvent, A is the absorbance at the excitation wavelength, and I is the integrated area under the corrected emission curve. The subscripts s and r refer to the sample and reference, respectively. A solution of quinine sulfate in 0.5 M H_2SO_4 (Φ_r = 54.6%) was used as external reference.[10] Circular dichroism measurements were performed at 298 K using a JASCO J-1000 instrument.

Circular Dichroism spectra (DCM solution)

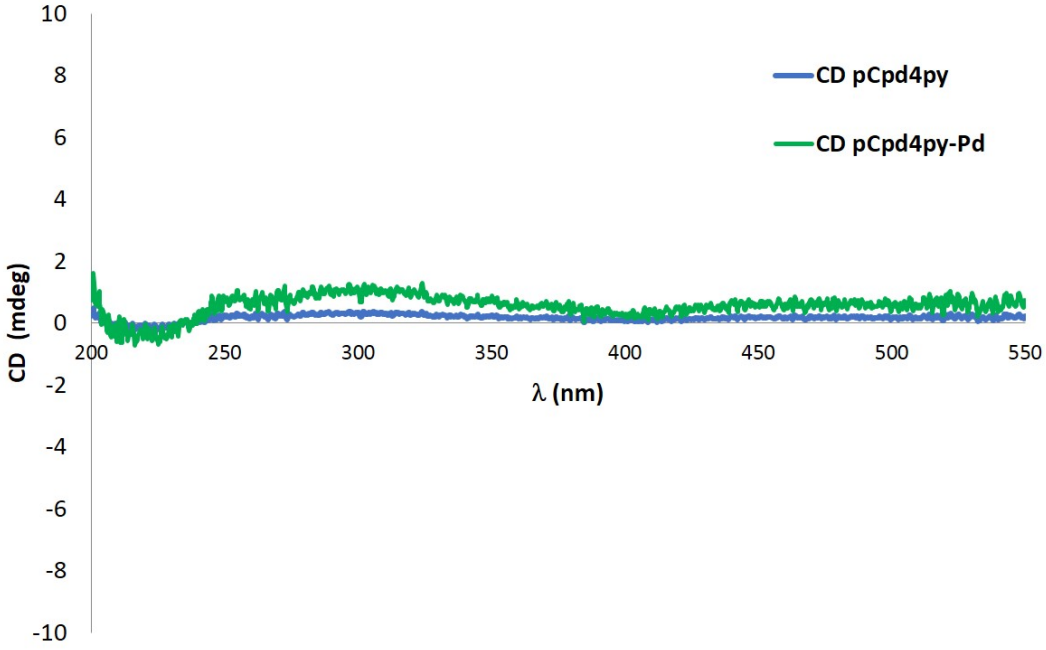

Figure **S17**. CD spectra of **pCpd4py** (blue line) and **pCpd4py-Pd** (green line) collected in DCM at 298 K at a concentration of 1 x 10^{-5} M.

UV-Vis absorption spectroscopy (DCM solution).

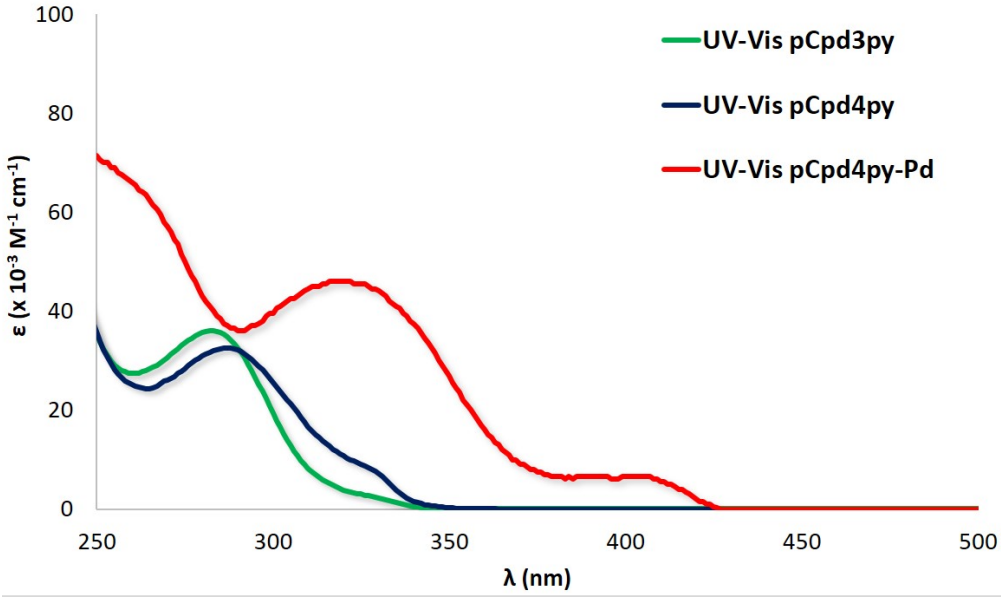

Figure **S18**. UV-Vis absorption spectra of **pCpd3py** (green line), **pCpd4py** (blue line) and **pCpd4py-Pd** (red line) collected in DCM at room temperature.

Table **S2**. UV-Vis absorption data of **pCpd3py**, **pCpd4py** and **pCpd4py-Pd**

Compound	λ_{max}[a] (nm) [ε (×10^{-3} M^{-1} cm^{-1})]
pCp3py	284 [39.0], 328 [2.5]
pCp4py	289 [32.4], 326 [8.7]
pCp4py-Pd	322 [46.1], 405 [6.5]

[a] UV-Vis absorption in DCM with a concentration in the order of 10^{-5} – 10^{-6}M collected at 298 K.

Emission spectroscopy (DCM solution).

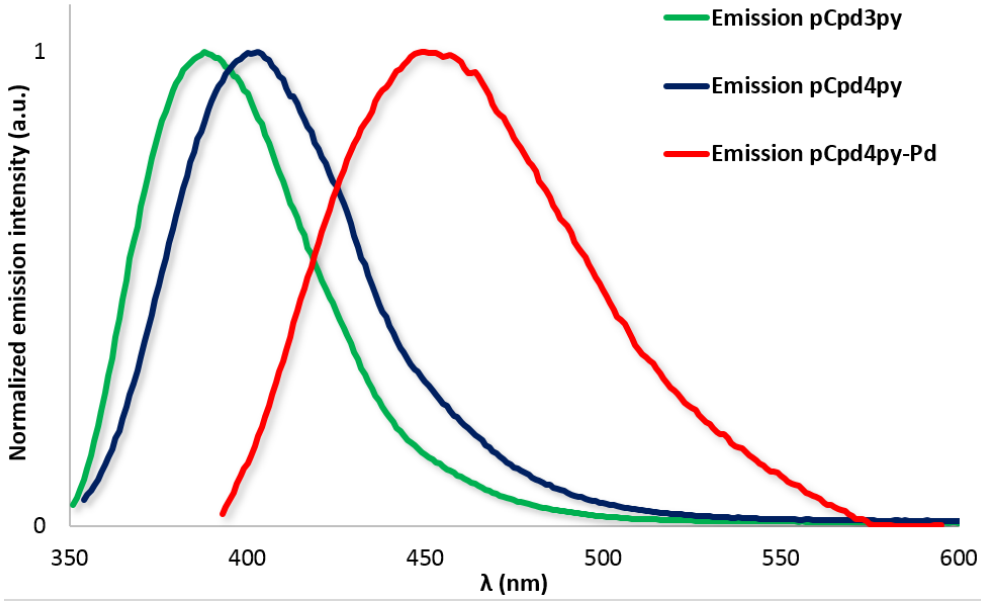

Figure **S19**. Normalized emission spectra of **pCpd3py** (green line), **pCpd4py** (blue line) and **pCpd4py-Pd** (red line) collected in degassed DCM at room temperature.

Emission spectroscopy(powder).

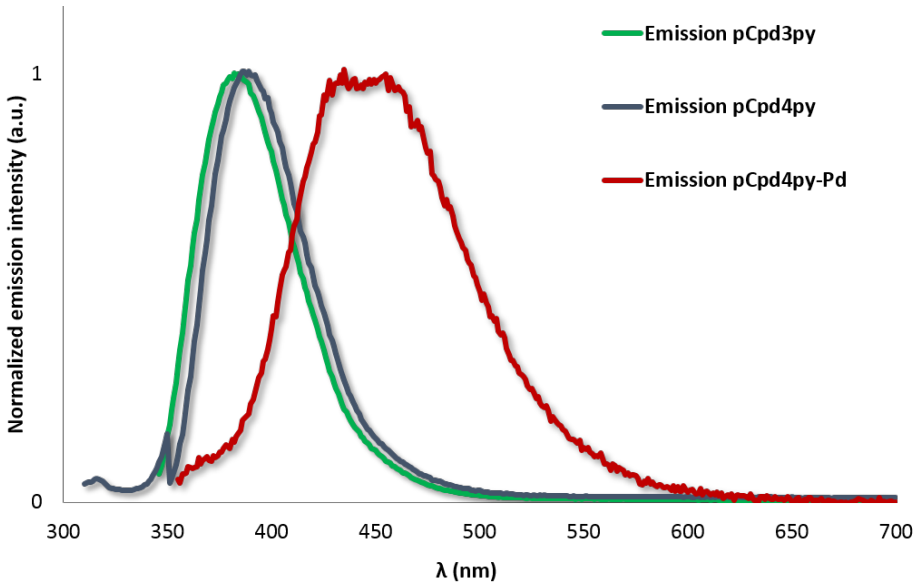

Figure **S20**. Normalized emission spectra of **pCpd3py** (green line), **pCpd4py** (blue line) and **pCp4py-Pd** (red line) collected as powders at room temperature.

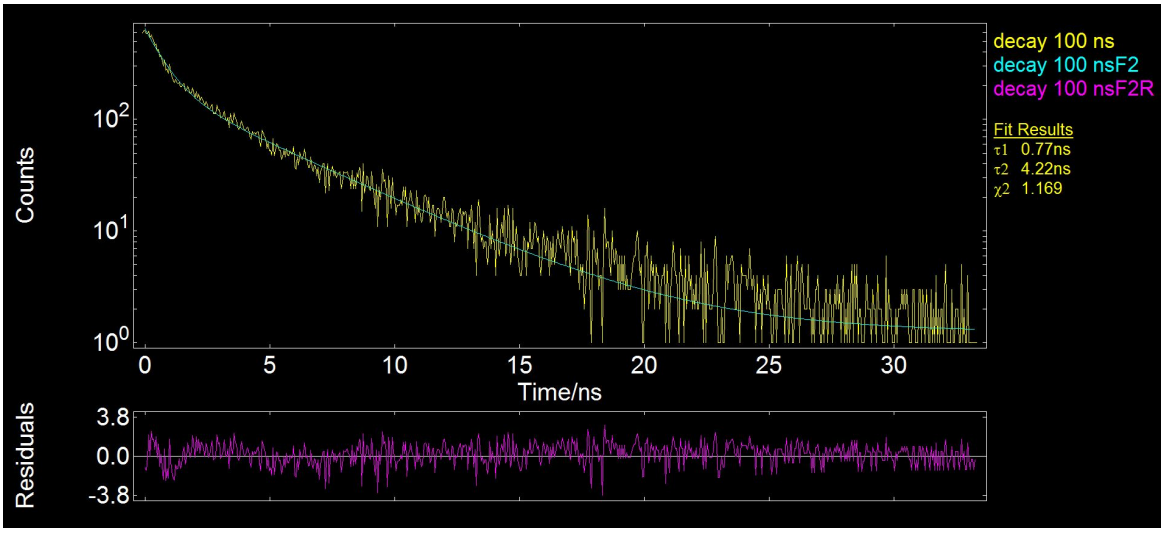

Figure **S21**. Lifetime decay of **pCpd3py** collected after excitation at 379 nm in degassed DCM solution at room temperature.

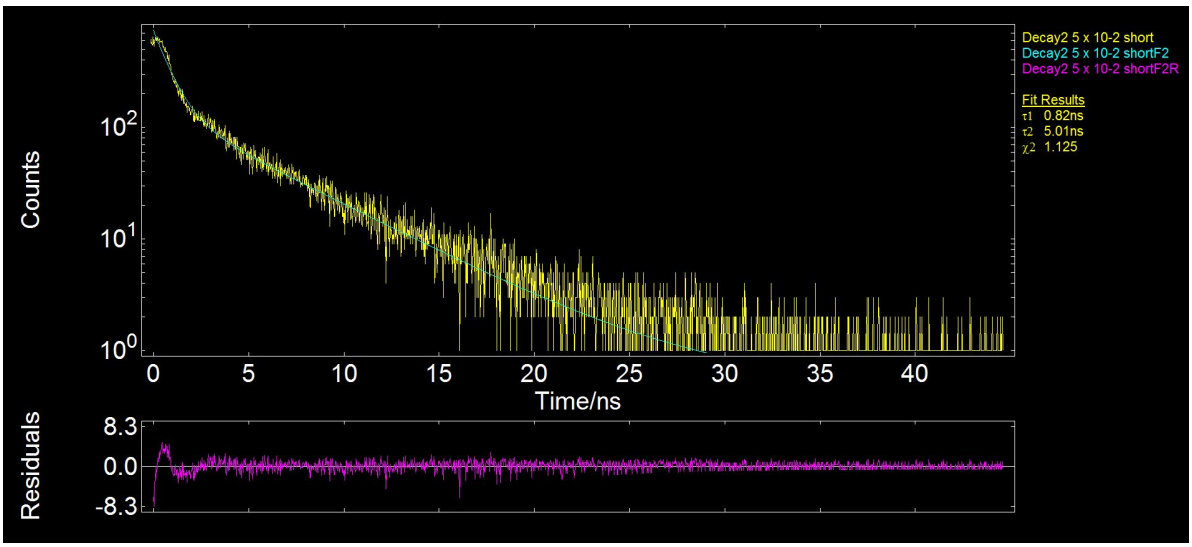

Figure **S22**. Lifetime decay of **pCpd4py** collected after excitation at 379 nm in degassed DCM solution at room temperature.

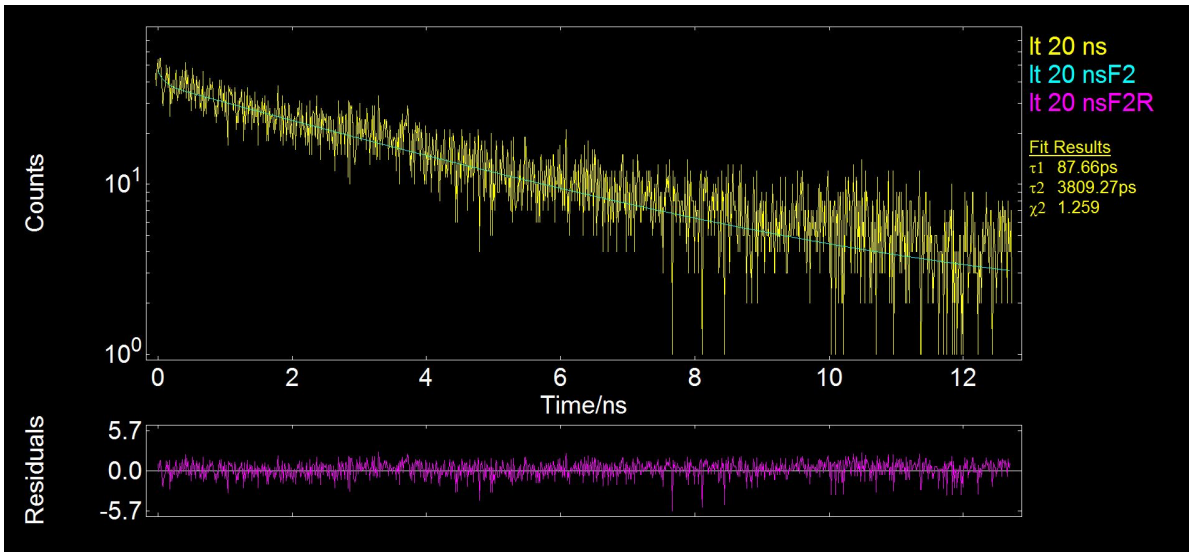

Figure **S23**. Lifetime decay of **pCpd4py-Pd** collected after excitation at 379 nm in degassed DCM solution at room temperature.

DFT and TD-DFT calculations.

Computational details

All theoretical calculations have been performed with the Gaussian16 code.[11] We have applied default algorithms, parameters and convergence thresholds, but for those detailed below. First, we have performed geometry optimizations using the PBE0[12] functional combined with the 6-31G(d) atomic basis set for all atoms, but for the metallic centers (Pd) that were modeled with the LanL2DZ basis set and pseudopotential. We applied the tightest possible DFT integration grid available in Gaussian 16, the so-called *superfine* grid and the solvent effects were accounted for using the Polarizable Continuum Model (PCM).[13] The transition energies to the lowest excited-states were determined using Time-Dependent Density Functional Theory (TD-DFT)[14] in combination with the same PBE0 functional[12] as well as the CAM-B3LYP[15] range-separated hybrid. During the TD-DFT calculations the solvent effects (DCM) were accounted for using the linear-response formalism of PCM in its *non-equilibrium* limit.[16]

Additional data

In Table **S3**, we report the transition energies determined with both PBE0 and CAM-B3LYP for the two ligands. As can be seen the general features of the various transitions are very similar with both functionals, although the CAM-B3LYP results are blue-shifted as compared to the PBE0 ones, a usual trend for a functional incorporating more *exact* exchange. The fact that the lowest-lying transition does not disappear when going from PBE0 to CAM-B3LYP hints that it is physically correct and not a spurious transition. We therefore discuss only the PBE0 results in the main text.

Table **S3**. Computed vertical absorption properties of **pCpd3py** and **pCpd4py**: vertical transition wavelength, oscillator strength, and dominant MO composition as obtained with PBE0 and CAM-B3LYP TD-DFT calculations.

	PBE0			**CAM-B3LYP**		
	λ/nm	f	MO	λ/nm	f	MO
pCpd3py	300	0.004	H — L (65%)	277	0.003	H — L (43%)
	287	0.140	H-1 L (74%)	261	0.217	H-1 L (56%)
	276	0.046	Mixed	258	0.042	H-2 L (56%)
	274	0.074	Mixed	252	0.100	H — L+1 (41%)
pCpd4py	306	0.003	H — L (88%)	281	0.003	H — L (67%)
	291	0.100	H-1 L (91%)	264	0.125	H-1 L (70%)
	280	0.098	H-2 L (44%)	261	0.129	H-2 L (38%)
	277	0.109	H-1 L+1 (67%)	253	0.105	Mixed

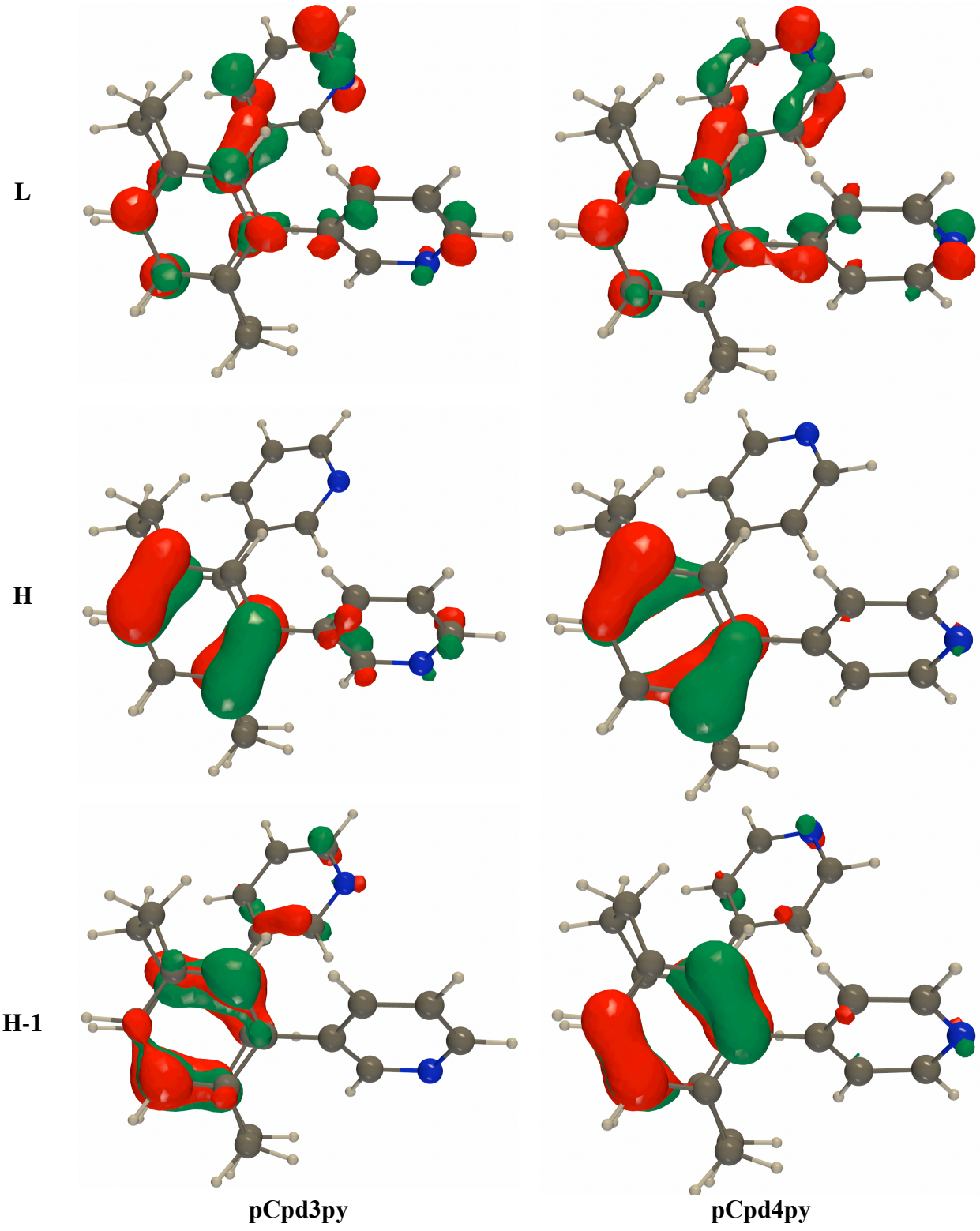

Figure **S24**. Selected PBE0 MOs for both **pCpd3py** and **pCpd4py**. Contour threshold: 0.05 au

In Table **S4**, we report the fifteen lowest transition energies determined with both PBE0 and CAM-B3LYP for cage. As for the separated ligands the key features are the same in both cases, that is a long list of weakly-allowed transitions significantly red-shifted as compared to the individual ligands. Due to the high symmetry of the cage, these transitions all involve a very complex mix of individual MO transitions. However, the relatively intense absorption at 377 and 376 nm (PBE0) all involve transitions from the from the eight highest occupied MOs to the three lowest unoccupied MOs. As an illustration the six frontier MOs are displayed in Figure **S25**, and their location as well as their degenerate character are clear.

Table **S4**. Computed vertical absorption properties of the **pCpd4py-Pd cage**: vertical transition wavelength and oscillator strength as obtained with PBE0 and CAM-B3LYP TD-DFT calculations.

PBE0		**CAM-B3LYP**	
λ/nm	f	λ/nm	f
392	0.000	396	0.000
391	0.001	396	0.000
391	0.001	396	0.001
378	0.003	331	0.017
377	0.001	330	0.024
377	0.013	330	0.026
377	0.030	324	0.000
376	0.004	323	0.001
376	0.026	322	0.002
370	0.016	320	0.045
370	0.002	320	0.030
370	0.015	320	0.032
368	0.002	319	0.010
368	0.005	317	0.086
368	0.019	317	0.081
368	0.012	311	0.004
367	0.012	310	0.004
366	0.003	310	0.006
365	0.012	305	0.150
365	0.008	304	0.030

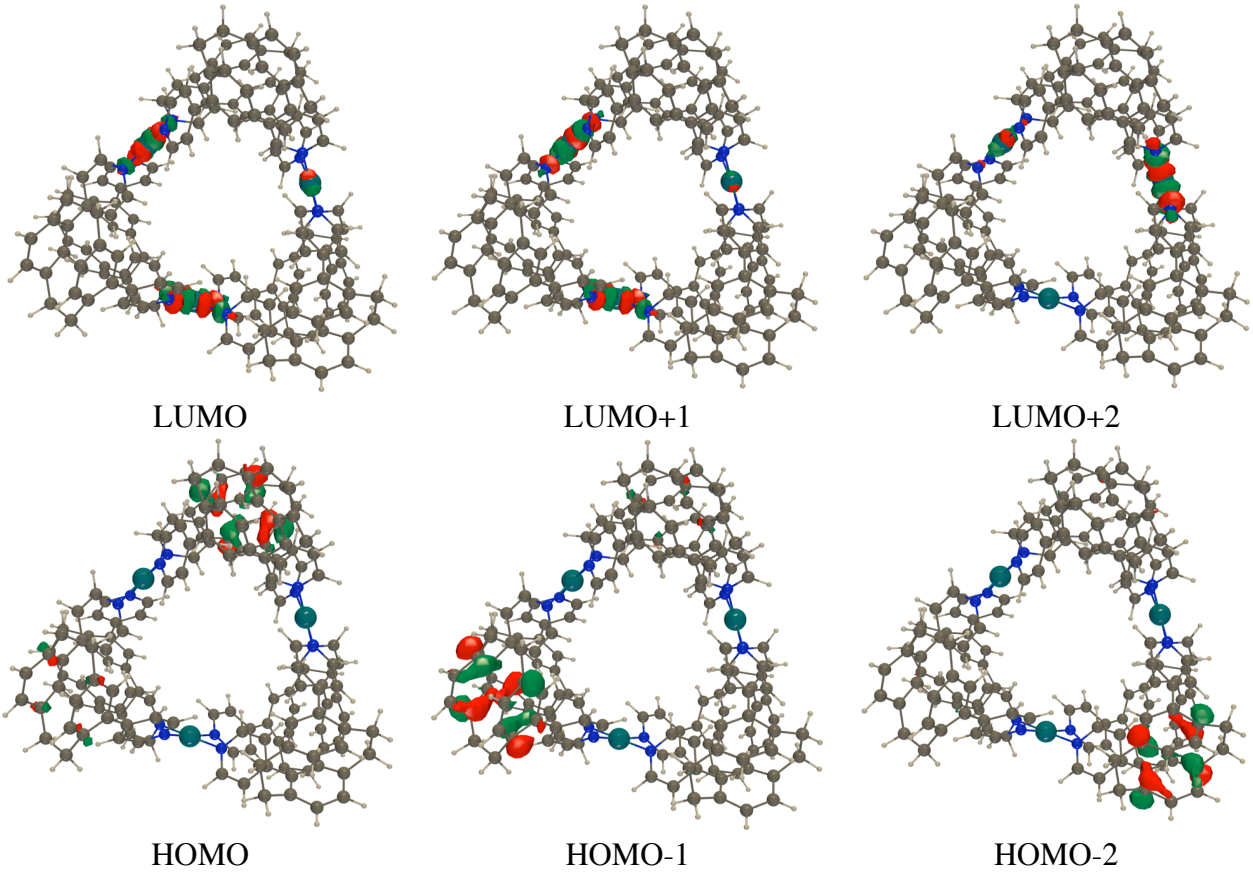

Figure **S25**. Frontier MOs for **pCpd4py-Pd**. Contour threshold: 0.05 au

References

[1] *CrystalClear-SM Exper*t v2.1. Rigaku Americas, The Woodlands, Texas, USA, and Rigaku Corporation, Tokyo, Japan, 2015

[2] *CrysAlisPro* v1.171.38.43i. Rigaku Oxford Diffraction, Rigaku Corporation, Oxford, U.K. 2015

[3] Burla, M. C.; Caliandro, R.; Camalli, M.; Carrozzini, B.; Cascarano, G. L.; Giacovazzo, C.; Mallamo, M.; Mazzone, A.; Polidori, G.; Spagna, R. *J. Appl. Cryst*. **2012**, *45*, 357-361

[4] Sheldrick, G. M. *Acta Crystallogr., Sect. A*. **2015**, *71*, 3-8

[5] Sheldrick, G. M. *Acta Crystallogr., Sect. C*. **2015**, *71*, 3-8

[6] Spek, A. L. *Acta Crystallogr. Sect C*. **2015**, *71*, 9-18

[7] Spek, A. L. *Acta Crystallogr. Sect D*. **2009**, *65*, 148-155

[8] *CrystalStructure* v4.3.0. Rigaku Americas, The Woodlands, Texas, USA, and Rigaku Corporation, Tokyo, Japan, 2018

[9] Crosby, G. A.; Demas, J. N. *J*. *Phys*. *Chem*. **1971**, *75*, 991

[10] Brouwer, A. M. *Pure Appl*. *Chem*. **2011**, *83*, 2213

[11] Frisch, M. J. et al., Gaussian 16, Rev. A.03, **2016**, Gaussian Inc. Wallingford, CT

[12] Adamo, C; Barone, V. *J. Chem. Phys.* **1999**, *111*, 2889

[13] Tomasi, J.; Mennucci, B; Cammi, R. *Chem. Rev.* **2005**, *105*, 2999

[14] Adamo, C.; Jacquemin, D. *Chem. Soc. Rev.* **2013**, *42,* 845

[15] Yanai, T.; Tew, D.; Handy, N. C. *Chem. Phys. Lett.* **2004**, *393*, 51

[16] Cammi, R. ; Mennucci, B. *J. Chem. Phys.* **1999**, *110*, 9877